Electronic Supplementary Material (ESI) for ChemComm.


# Supplementary Information for

# $[Zr_6O_4(OH)_4(benzene\text{-}1,4\text{-}dicarboxylato)_6]_n$: a hexagonal polymorph of UiO-66

Maite Perfecto-Irigaray,[a] Garikoitz Beobide,*[a] Oscar Castillo,*[a] Ivan da Silva,[b] Daniel García-Lojo,[a] Antonio Luque,[a] Ander Mendia,[a] and Sonia Pérez-Yáñez[ac]

[a] *Departamento de Química Inorgánica, Facultad de Ciencia y Tecnología, Universidad del País Vasco/Euskal Herriko Unibertsitatea, UPV/EHU, Apartado 644, E-48080 Bilbao, Spain.*
[b] *ISIS Facility, STFC Rutherford Appleton Laboratory, Chilton, Oxfordshire OX11 0QX, U.K.*
[c] *Departamento de Química Inorgánica, Facultad de Farmacia, Universidad del País Vasco/Euskal Herriko Unibertsitatea, UPV/EHU, E-01006 Vitoria-Gasteiz, Spain.*

## S0. PHYSICAL MEASUREMENTS

## S0. PHYSICAL MEASUREMENTS

Routine **powder X-ray diffraction** (**PXRD**) measurements were performed on a Phillips X'PERT diffractometer (equipped with Cu-Kα radiation, λ = 1.5418 Å) over the range $5 < 2\theta < 70^{o}$ with a step size of $0.02^{o}$, a variable automatic divergence slit and an acquisition time of 2.5 s per step at 293 K.

**Variable temperature PXRD** data were collected on a Bruker D8 Advance diffractometer operating at 30 kV and 20 mA, equipped with a Cu tube (λ = 1.5418 Å), a Vantec-1 PSD detector, and an Anton Parr HTK2000 high-temperature furnace. The powder patterns were recorded in the 5–38° 2θ range using steps of 0.033 $^{o}$ and 1 s per step. Data sets were recorded in air atmosphere each 10 $^{o}$C from 30 to 500 $^{o}$C, using a heating rate of 0.166 $^{o}$C $s^{-1}$.

**Fourier-transform infrared** (**FTIR**) spectra of the samples (KBr pellet) were recorded at a resolution of 4 $cm^{-1}$ in the 4000–500 $cm^{-1}$ region using a FTIR 8400S Shimadzu spectrometer.

**Thermal analysis** (**TGA**) was performed on a METTLER TOLEDO TGA/SDTA851 thermal analyser in synthetic air (80% $N_2$, 20 %$O_2$) flux of 50 $cm^3 \cdot min^{-1}$, from room temperature to 800 °C with heating rate of 5 °C $min^{-1}$ and a sample size of about 10–20 mg per run.

**Transmission electron microscopy** (**TEM**) studies were carried out on a JEOL JSM-7000F microscope operated at 10-20 kV and coupled with an energy dispersive X-ray spectrometer (EDX). Specimens were mounted on conductive carbon adhesive tabs and sputtered with a 5 nm chromium coating to make them conductive.

Dinitrogen (77 K) and carbon dioxide (273 and 298 K) **physisorption data** were recorded with a Quantachrome Autosorb-iQ MP. Prior to measurements all samples were thoroughly washed with *N,N*-dimethylformamide (DMF) and methanol (MeOH) to remove the remaining reagents from the pore, and thereafter, outgassed under vacuum at 140 °C for 5 hours.

**Gas chromatography–mass spectrometry (GC-MS)** measurements were performed on an Agilent HP 6890 gas chromatograph coupled to a mass spectrometer Agilent, HP5973 to analyse the formation of sub-products during the synthesis of EHU-30. Accordingly, a liquid-solid extraction was carried out on the doughy reaction product using methanol as solvent (0.05:1) mass ratio, afterwhich, aliquots of 1 µL were taken and injected on the spectrometer. A HP 5 MS chromatography column was employed, with helium as gas carrier and a flux of 1.3 $mL \cdot min^{-1}$. The injection was done in split mode at 300 $^{o}$C, and the temperature of the oven was heated up from 60 $^{o}$C to 300 $^{o}$C with a heating rate of 15 $^{o}C \cdot min^{-1}$.

**$^{1}$H-NMR spectra** were acquired in a Bruker AVANCE 5OO (one-bay; 500 MHz) at 293 K.

## S1. SYNTHESIS AND CHEMICAL CHARACTERIZATION

## S1. SYNTHESIS AND CHEMICAL CHARACTERIZATION

**Chemicals**. All the chemicals were of reagent grade and were used as commercially obtained.

**Synthesis**. The general procedure to synthesize EHU-30 was accomplished as follows: zirconium(IV) propoxide (Sigma-Aldrich, 70% wt in 1-propanol; 1.0529 g, 2.25 mmol) was mixed under continuous stirring with methacrylic acid (Sigma-Aldrich, 99%, 1.015 $g \cdot cm^{-3}$; 700 μL, 8.17 mmol) and benzene-1,4-dicarboxylic acid (Sigma-Aldrich, 98%; 0.3814 g, 2.25 mmol). Thereafter, the flask was sealed and the resulting doughy reaction mixture was heated upon 140 °C for 90 minutes. The synthesis product was thoroughly washed with methanol and dried under ambient conditions. The resulting compound exhibited the aspect of a finely divided white powder.

It deserves to note that the water (or hydroxide/oxide anions) required for the formation of the zirconium cluster is produced by a side reaction that involves the partial esterification of the carboxylic acids with the propanol/propanoate contained in the Zr(IV) reagent (see Figure S1.1a). The presence of the esterification products, propyl methacrylate (propyl 2-methylprop-2-enoate) and propyl benzene-1,4-dicarboxylate, was verified by GC-MS measurements (Figure S1.1b). It must be considered that previous works have demonstrated the capability of Zr(IV) complexes (including MOFs) to catalyse etherification and esterification reactions.[1]

In any case, the addition of 10 μL of water ensures the reproducibility of the synthesis in terms of crystallinity and adsorptive performance. No additional solvent was employed to coerce the interaction between the methacrylic acid and the growing metal-organic skeleton. In fact, the increase of the added water amount prompts the formation of scarcely crystalline UiO-66 phase, as it can be seen in Figure S1.2.

The chemical characterization of EHU-30 was completed by infrared spectroscopy, $^{1}$H-NMR, thermogravimetric analysis, variable-temperature PXRD and transmission electron microscopy (see Figures S1.3-S1.7). Prior to measurements the samples were outgassed under vacuum (140 °C, 6 h) to remove solvent molecules that might interfere in the chemical analyses.

[1] (a) D. Yang, M. A. Ortuño, V. Bernales, C. J. Cramer, L. Gagliardi and B. C. Gates, *J. Am. Chem. Soc.,* 2018, **140**, 3751; (b) F. G. Cirujano, A. Corma and F. X. Llabrés i Xamena, *Catalysis Today*, 2015, **257**, 213.

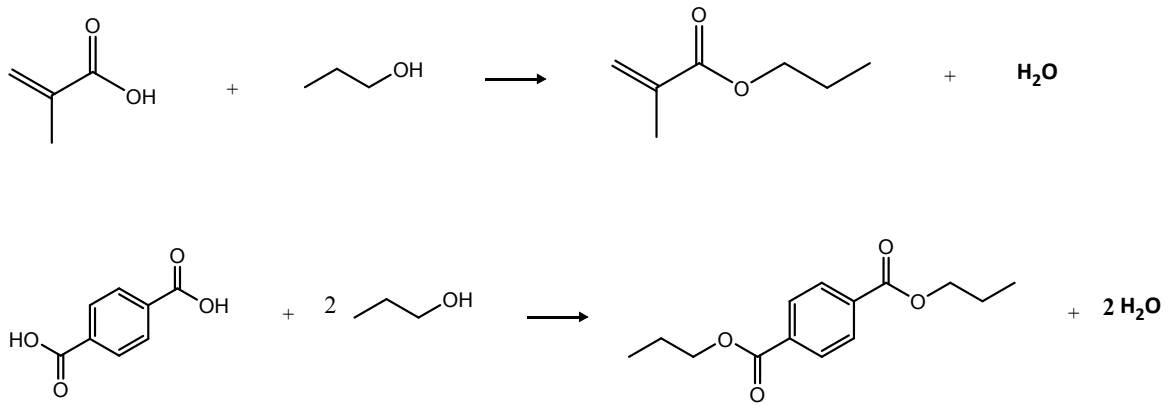


(a)

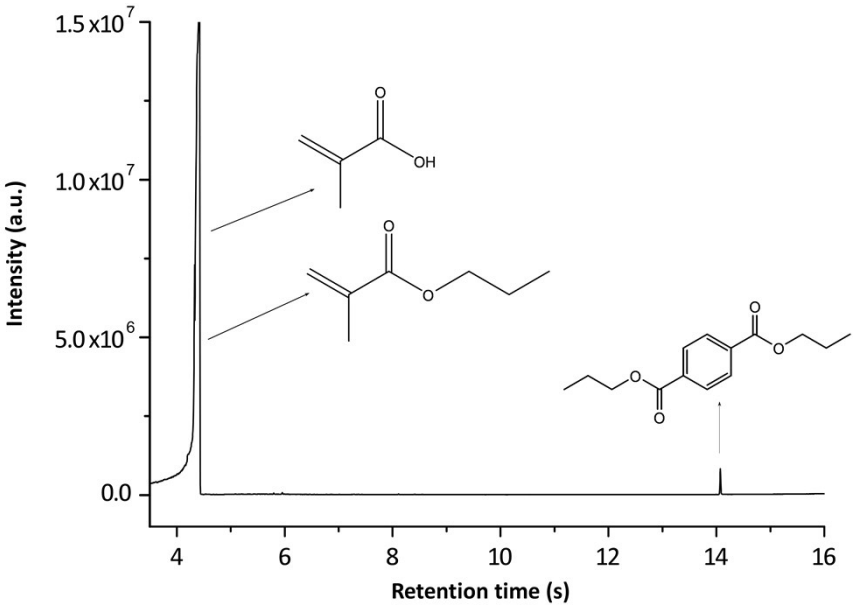


(b)

**Figure S1.1.** (a) Reaction schemes for the esterification of the carboxylic acids that take place during the synthesis process of EHU-30. (b) Chromatogram (GC-MS) taken on the leachate of the reaction product, in which the propyl esters of methacrylic acid and benzene-1,4-dicarboxylic acid were identified.

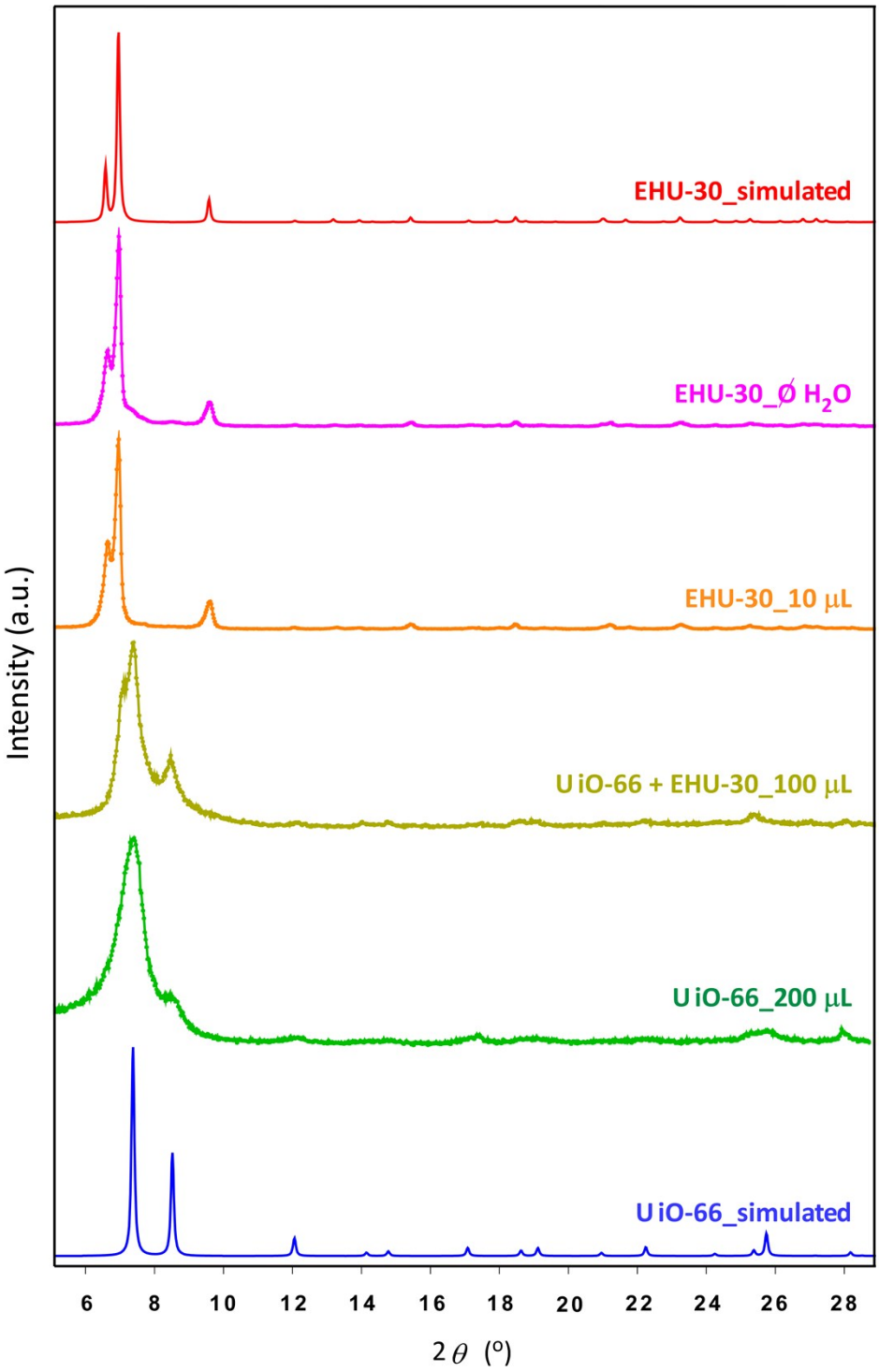


**Figure S1.2.** Experimental PXRD patterns for samples synthesised with varying amount of water and simulated PXRD patterns for EHU-30 and UiO-66.

The infrared spectrum of EHU-30 and the assignation of the vibration modes are gathered in Figure S1.3. The large O-H peaks in the IR spectrum is indicative of $H_2O/OH^-$ pairs replacing missing linkers in the structure (see below further details in thermogravimetric analysis).

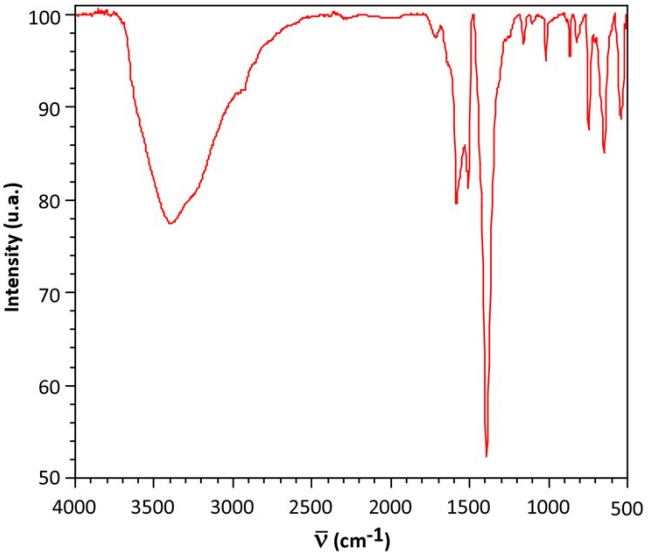


(a)

| $\bar{\nu}$ (cm$^{-1}$) | |
|---|---|
| 3320 | $\nu$ (O-H) |
| 1700 | $\nu$ (C=O) |
| 1580 | $\nu$ (C-C) |
| 1400 | $\nu$ $(O\text{-}C\text{-}O)_s$ + $\nu$ $(C\text{-}C)_{ar}$ |
| 1016 | $\delta_{ip}$ (C-H) |
| 745 | $\delta_{oop}$ (C-H) + $\delta_{oop}$ (O-C-O) |
| 659 | $\nu$ $(Zr\text{-}O^{2-})$ |
| 548 | $\nu$ $(Zr\text{-}O_{carboxylato})$ |

(b)

**Figure S1.3.** (a) FTIR spectrum and (b) band assignments for EHU-30 (*s* = symmetric, *ar* = aromatic, *ip* = in plane, *oop* = out of plane).

To proceed with the $^1$H-NMR spectrum (500 MHz), a 20 mg sample of EHU-30 was digested in 600 µL of a 1 M NaOH solution (in deuterated water, $D_2O$). The digestion was prolonged for 24 h, after which the solid residue corresponding to $ZrO_2$ was filtered off and the NMR spectrum was taken on the liquid fraction (Figure S1.4). The residual signal of the solvent appears at 4.79 ppm, while a singlet at 7.84 ppm is due to the aromatic signals of benzene-1,4-dicarboxylic acid. Extending the area around 5.0 ppm, the two characteristic singlets of the olefinic protons of methacrylic acid (5.61 and 5.30 ppm) are found. Besides, at 1.83 the signal corresponding to the methyl group of the methacrylic acid (which integrates 3:1 regarding the methylene group) can be observed. The integration of the respective signals shows that the amount of methacrylic acid after the digestion of the MOF is of a 6% relative to benzene-1,4-dicarboxylic acid which fits fairly well that estimated from the TGA analysis (see below).

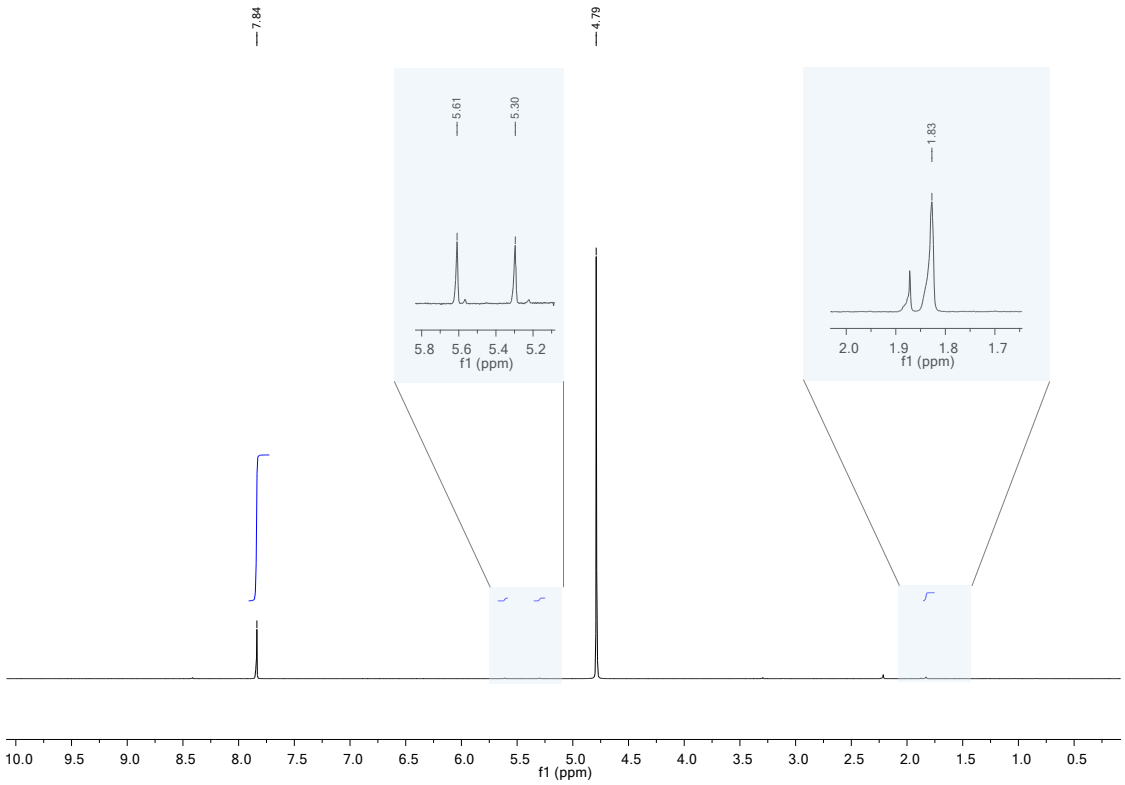


(a)

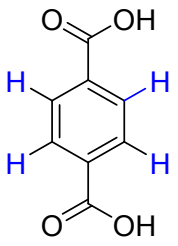


δ (H) = 7.84 ppm

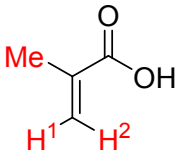


δ ($H^1$)= 5.30 ppm
δ ($H^2$)= 5.61 ppm
δ (Me)= 1.83 ppm

(b)

**Figure S1.4.** (a) $^1$H-NMR spectrum of digested EHU-30 sample. (b) Signals corresponding to benzene-1,4-dicarboxylic acid and methacrylic acid.

Thermogravimetric analysis shows a similar behaviour to that found for other zirconium based MOFs. There are three weight losses that have been typically assigned to the following processes:

(1) *ca.* 25 – 130 °C range: $H_2O$ release

(2) *ca.* 200 – 350 °C range: removal of monocarboxylate ligands (this loss is accompanied by a small exothermic peak) and dehydroxilation of the $Zr_6$ cluster. These two weight losses are not well-resolved from one another.

(3) *ca.* 390 – 525 °C range: framework decomposition. This loss is accompanied by a very intense exothermic peak.

In order to provide a more precise formula, we calculated the number of linker deficiencies per $Zr_6$ formula unit from the thermogravimetric analysis. Among the previously described three possibilities of defect compensating ligands (chloride, $OH^-/H_2O$ and monocarboxylates) we can state that in our compound two of them are present, which has been corroborated by $^1$H-NMR spectra and ATR-IR results.

In good agreement with those data, we can propose, from the thermogravimetric analysis, the following formula: $[Zr_6(OH)_4O_4(C_8H_4O_4)_{5.00}(C_4H_5O_2)_{0.32}(H_2O)_{1.68}(OH)_{1.68}]_n$ (MW: 1586.01 g/mol), in which a small fraction of benzene-1,4-dicarboxylato ligands has been replaced by methacrylato ligands and $OH^-/H_2O$ pairs.

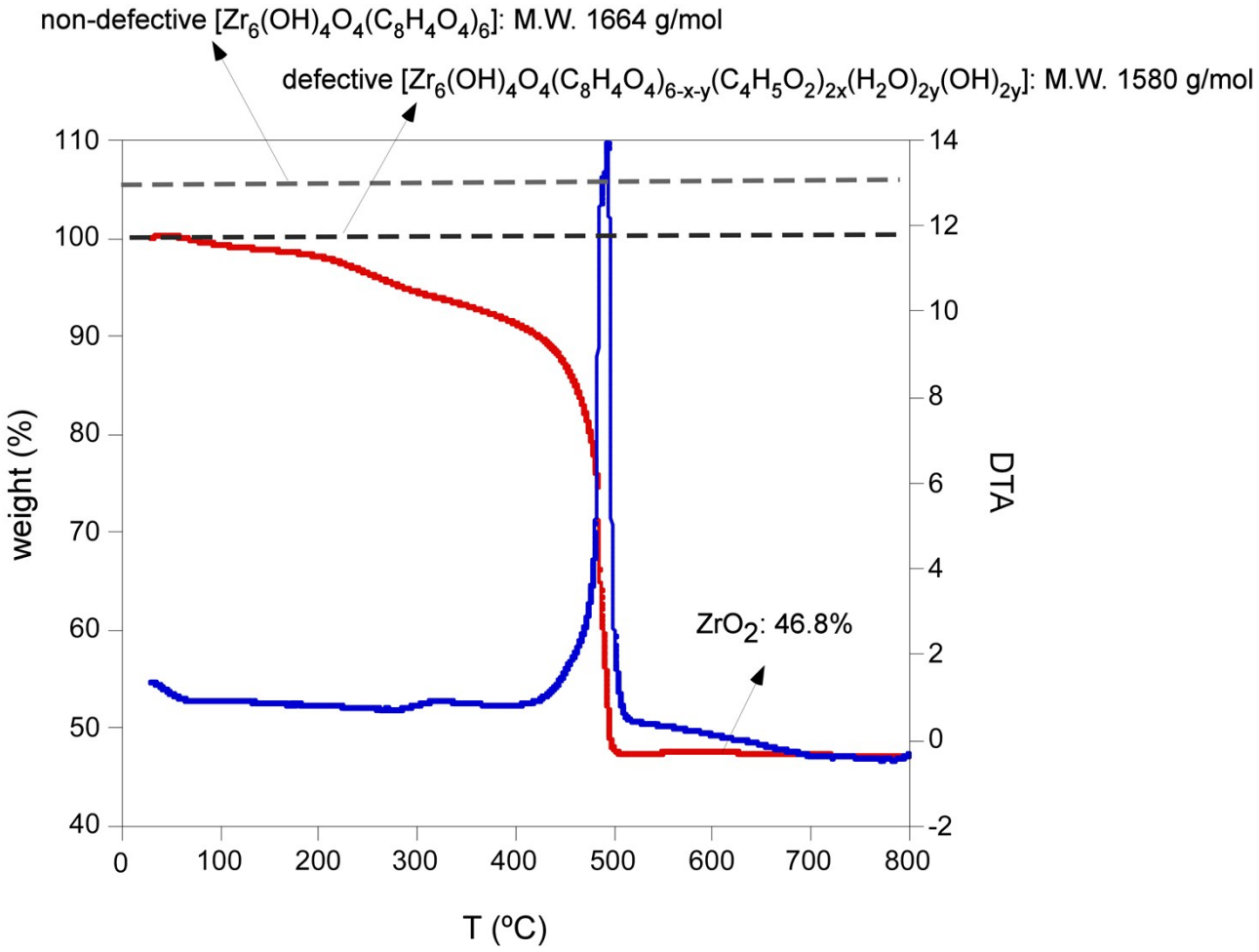


**Figure S1.5.** TGA-DTA curves of EHU-30.

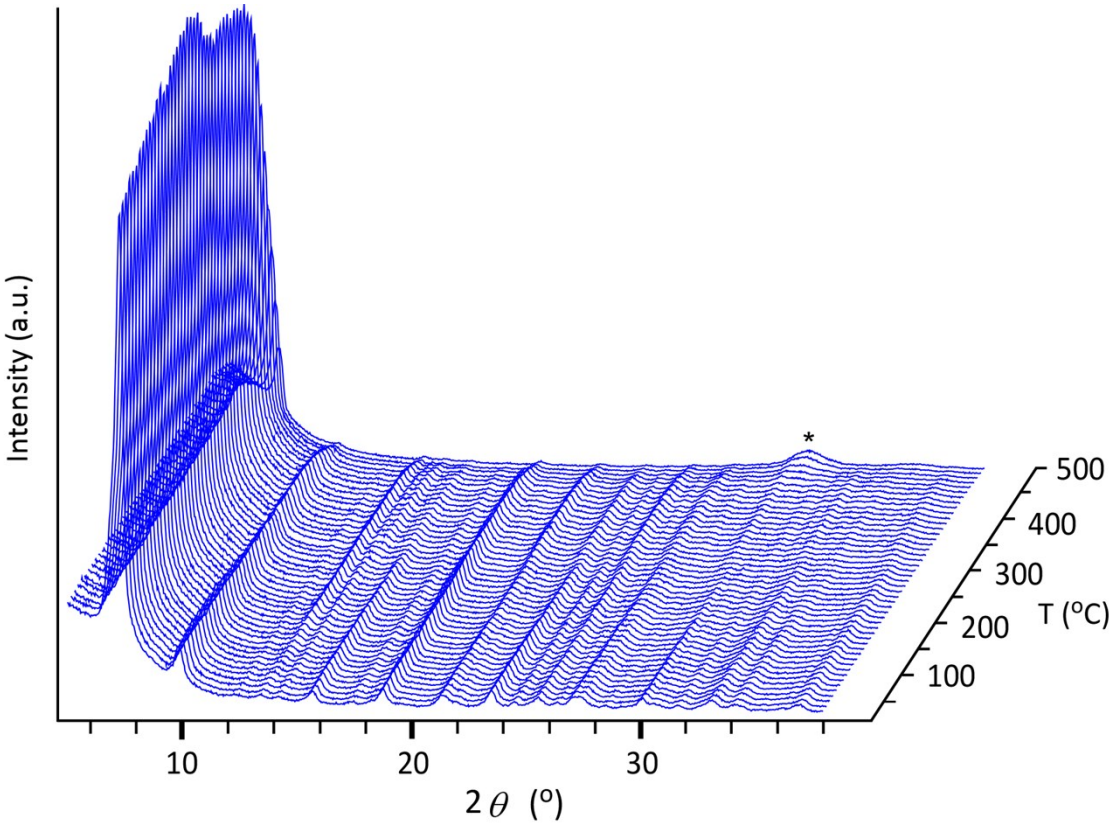


**Figure S1.6.** Variable-temperature PXRD patterns of EHU-30 measured from 20 to 500 °C at air atmosphere. Asterisk mark corresponds to the formation of $ZrO_2$ that results from the degradation of EHU-30.

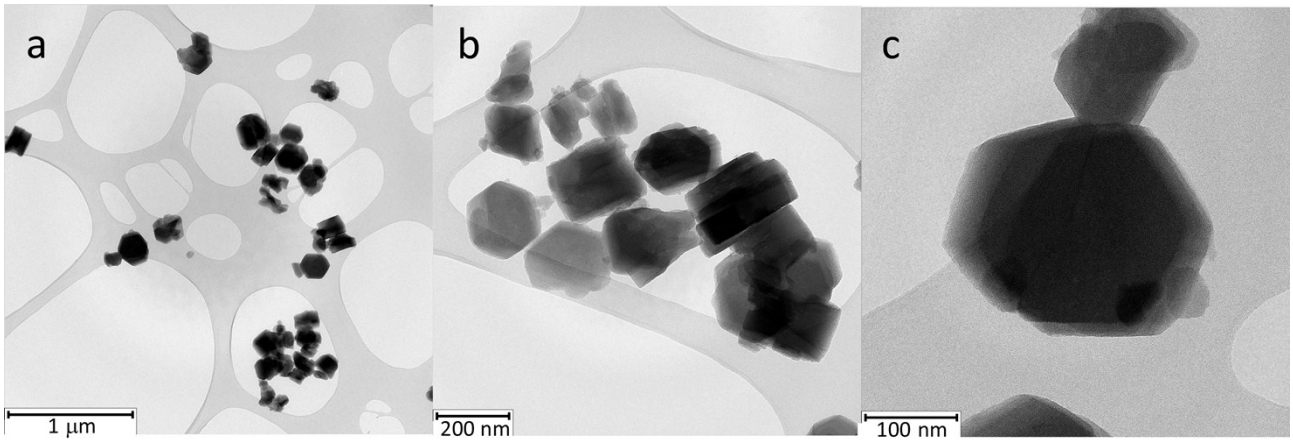


**Figure S1.7.** Transmission electron microscopy images taken on EHU-30.

## S2. SYNCHROTRON DATA COLLECTION AND CRYSTAL STRUCTURAL ELUCIDATION

## S2. SYNCHROTRON DATA COLLECTION AND CRYSTAL STRUCTURAL ELUCIDATION

High resolution synchrotron X-ray diffraction pattern of polycrystalline EHU-30 was measured at I11 Beamline of Diamond Light Source equipped with a multi-analyser crystal detector (MAC) and using a wavelength of λ = 0.82448(10) Å.[2] The sample was mounted in a borosilicate capillary and outgassed at 353 K under vacuum. After cooling down to room temperature, the capillary was thermally sealed. PXRD data was collected at 293 K.

The peak search algorithm implemented in Topas v5 program[3] was used to determine the angular positions of the first 42 reflections (up to about 20° 2θ). These positions were used to index the pattern using Topas v5 program into the hexagonal system. EXPO2004 program[4] was used for the space-group determination procedure. This software determines the most probable extinction group by means of a statistical algorithm.[5] The figure of merits[6] for the space group search are gathered in Table S2.1. The highest probability was assigned to extinction group *P* - - *c*. The two following ranked extinction groups were *P* $6_3$ - - and *P* $6_1$ - -. From the five different space groups compatible with the reflection conditions of extinction group *P* - - *c* (i.e. *P*-31*c*, *P*31*c*, *P*-62*c*, *P*$6_3$/*mmc* and *P*$6_3$*mc*), *P*$6_3$/*mmc* presents the higher number of symmetry operators, so it was chosen for the crystal structure solution process. As stated, the highest symmetry with a reasonable factor of merit (FoM) belonged to *P*$6_3$/*mmc*, which imposes the corresponding symmetry restraints on the crystal structure. No additional symmetry restraints have been applied. Crystal structure solutions using lower symmetry space groups give rise an undistinguishable result.

Crystal structure of EHU-30 was solved *ab initio* using Topas v5 program. Firstly, crystallographic position of heavy atom Zr was found by using the Charge–Flipping method[7,8]. Using only the Zr atom position, a preliminary Rietveld refinement[9] was carried out. This allowed calculating a difference Fourier map, which clearly showed electron density peaks, corresponding to atoms O1 and O2 of the Zr-based cluster. After including these two atoms in the Rietveld refinement, a subsequent different Fourier map already showed electron density clouds connecting the clusters, which corresponded to the organic linkers. These were then described in the refinement as semi-rigid body units.

Final Rietveld refinement of EHU-30 crystal structure was carried out in the 2θ range from 2.5 to 65° (about 0.77 Å in *d*-spacing) and atomic coordinates of all atoms were included. Different isotropic temperature factors were introduced for the organic linkers, O1 and O2 atoms and Zr atom in the structure refinement. The peak function used for fitting the experimental data was the Thompson–Cox–Hastings Pseudo–Voigt[10]; a 36 coefficients Chebyshev polynomial was used to model the background. On the final Rietveld fit, there were 90 different adjustable parameters (scale factor, zero shift, unit-cell parameters, peak-shape parameters, atomic coordinates and temperature factors). In Figure S2.1, the plot of the final Rietveld fit for EHU-30 compound is given. Table S2.2 reports crystallographic and refinement-related data, while atomic coordinates for non-H atoms are reported in Table S2.3.

[2] S. P. Thompson, J. E. Parker, J. Potter, T. P. Hill, A. Birt, T. M. Cobb, F. Yuan and C. C. Tang, *Rev. Sci. Instrum.*, 2009, **80**, 075107.

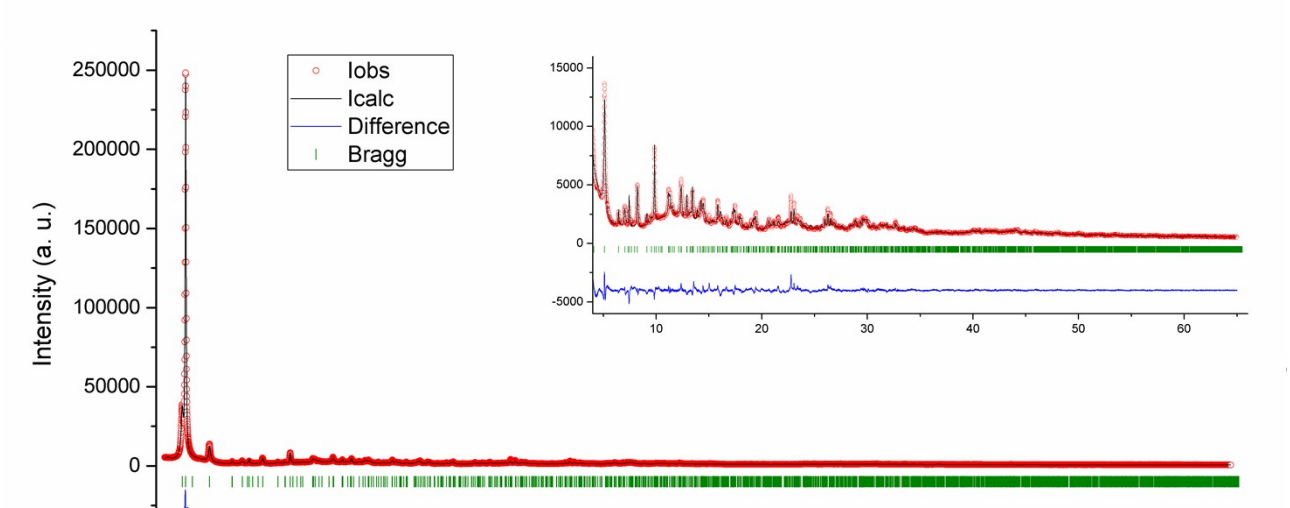

**Figure S2.1.** Final Rietveld refinement plot for EHU-30, showing the experimental (red circles), calculated (black line), and difference profiles (blue line); green tick marks indicate reflection positions. The inset shows a magnification of the peaks after the most intense one.

**Table S2.1.** Figure of merits for the space group search for EHU-30.

| **Space Group** | **Extinction Symbol** | **FoM** |
|---|---|---|
| *P* -3 1 c | *P* _ _ *c* | 0.522 |
| *P* 3 1 c | *P* _ _ *c* | 0.522 |
| *P* -6 2 c | *P* _ _ *c* | 0.522 |
| *P* $6_3$/*m m c* | *P* _ _ *c* | 0.522 |
| *P* $6_3$ *m c* | *P* _ _ *c* | 0.522 |
| *P* $6_3$/*m* | *P* $6_3$ _ _ | 0.259 |
| *P* $6_3$ | *P* $6_3$ _ _ | 0.259 |
| *P* $6_3$ 2 2 | *P* $6_3$ _ _ | 0.259 |
| *P* $6_1$ | *P* $6_1$ _ _ | 0.063 |
| *P* $6_5$ | *P* $6_1$ _ _ | 0.063 |
| *P* $6_1$ 2 2 | *P* $6_1$ _ _ | 0.063 |
| *P* $6_5$ 2 2 | *P* $6_1$ _ _ | 0.063 |
| *P* $6_2$ | *P* $6_2$ _ _ | 0.052 |
| *P* $6_2$ 2 2 | *P* $6_2$ _ _ | 0.052 |
| *P* $6_4$ | *P* $6_2$ _ _ | 0.052 |
| *P* $6_4$ 2 2 | *P* $6_2$ _ _ | 0.052 |
| *P* $3_1$ 2 1 | *P* $3_1$ _ _ | 0.052 |
| *P* $3_1$ | *P* $3_1$ _ _ | 0.052 |
| *P* $3_2$ | *P* $3_1$ _ _ | 0.052 |
| *P* $3_2$ 2 1 | *P* $3_1$ _ _ | 0.052 |
| *P* $3_1$ 1 2 | *P* $3_1$ _ _ | 0.052 |
| *P* $3_2$ 1 2 | *P* $3_1$ _ _ | 0.052 |
| *P* -3 | *P* _ _ _ | 0.047 |
| *P* 3 | *P* _ _ _ | 0.047 |

| | | |
|---|---|---|
| *P* 3 2 1 | *P* _ _ _ | 0.047 |
| *P* -3 *m* 1 | *P* _ _ _ | 0.047 |
| *P* 6/*m m m* | *P* _ _ _ | 0.047 |
| *P* -6 *m* 2 | *P* _ _ _ | 0.047 |
| *P* -6 2 *m* | *P* _ _ _ | 0.047 |
| *P* 6 2 2 | *P* _ _ _ | 0.047 |
| *P* 6 *m m* | *P* _ _ _ | 0.047 |
| *P* -3 1 *m* | *P* _ _ _ | 0.047 |
| *P* 6/*m* | *P* _ _ _ | 0.047 |
| *P* -6 | *P* _ _ _ | 0.047 |
| *P* 3 1 *m* | *P* _ _ _ | 0.047 |
| *P* 3 1 2 | *P* _ _ _ | 0.047 |
| *P* 3 *m* 1 | *P* _ _ _ | 0.047 |
| *P* 6 | *P* _ _ _ | 0.047 |
| *P* 6/*m c c* | *P* _ *c c* | 0.042 |
| *P* 6 *c c* | *P* _ *c c* | 0.042 |
| *P* -3 *c* 1 | *P* _ *c* _ | 0.021 |
| *P* 3 *c* 1 | *P* _ *c* _ | 0.021 |
| *P* $6_3$/*m c m* | *P* _ *c* _ | 0.021 |
| *P* $6_3$ *c m* | *P* _ *c* _ | 0.021 |
| *P* -6 c 2 | *P* _ *c* _ | 0.021 |
| *R* -3 | *R* (obv) _ _ | 0.000 |
| *R* 3 | *R* (obv) _ _ | 0.000 |
| *R* 3 2 | *R* (obv) _ _ | 0.000 |
| *R* -3 *m* | *R* (obv) _ _ | 0.000 |
| *R* 3 *m* | *R* (obv) _ _ | 0.000 |
| *R* -3 | *R* (rev) _ _ | 0.000 |
| *R* 3 | *R* (rev) _ _ | 0.000 |
| *R* 3 2 | *R* (rev) _ _ | 0.000 |
| *R* -3 *m* | *R* (rev) _ _ | 0.000 |

| | | |
|---|---|---|
| *R* 3 *m* | *R* (rev) _ _ | 0.000 |
| *R* -3 *c* | *R* (obv) _ *c* | 0.000 |
| *R* 3 *c* | *R* (obv) _ *c* | 0.000 |
| *R* -3 *c* | *R* (rev) _ *c* | 0.000 |
| *R* 3 *c* | *R* (rev) _ *c* | 0.000 |

**Table S2.2.** Crystallographic data and Rietveld refinement summary for EHU-30.

| Compound | **EHU-30** |
|---|---|
| Formula | $[Zr_6(C_8H_4O_4)_6(O)_4(OH)_4]$ |
| Formula weight (g/mol) | 1664.06 |
| $D_c$ (g/cm$^3$) | 1.105 |
| Crystal system | Hexagonal |
| Space group | $P6_3/mmc$ |
| *a* (Å) | 14.6690(4) |
| *c* (Å) | 26.8478(19) |
| V (Å$^3$) | 5003.1(5) |
| *Z* | 2 |
| Radiation type | Synchrotron |
| Diffractometer | I11 Beamline, Diamond Light Source |
| Data collection mode | Transmission |
| Wavelength (Å) | 0.82448 |
| $R_p$ (%) | 5.13 |
| $R_{wp}$ (%) | 7.00 |
| $R_{exp}$ (%) | 1.68 |
| $R_B$ (%) | 3.41 |
| *Goodness-of-fit* | 4.17 |

**Table S2.3.** Fractional atomic coordinates and isotropic displacement parameter (Å$^2$) of non-H atoms for EHU-30.

| Atom | *x* | *y* | *z* | $B_{iso}$ |
|---|---|---|---|---|
| Zr1 | 0.8400(3) | -0.08001(14) | 0.05458(16) | 1.29(7) |
| O1 | 0.8321(14) | -0.0840(7) | -0.0274(8) | 0.5(4) |
| O2 | 1 | 0 | 0.0866(16) | 0.5(4) |
| C1 | 0.5282(7) | -0.0392(12) | 0.0414(9) | 7.2(4) |
| C2 | 0.597(3) | 0 | 0 | 7.2(4) |
| C3 | 0.699(3) | 0 | 0 | 7.2(4) |
| O3 | 0.723(3) | -0.0350(12) | 0.0371(10) | 7.2(4) |
| C4 | 0.812(15) | -0.21(3) | 0.2245(10) | 7.2(4) |
| C5 | 0.8935(17) | -0.213(3) | 0.199(2) | 7.2(4) |
| C6 | 0.9019(17) | -0.196(3) | 0.1454(19) | 7.2(4) |
| O4 | 0.84(2) | -0.17(3) | 0.124(4) | 7.2(4) |

## S3. CRYSTAL STRUCTURE COMPARATIVE VIEWS FOR EHU-30 AND UIO-66

## S3. CRYSTAL STRUCTURE COMPARATIVE VIEWS FOR EHU-30 AND UIO-66

| **EHU-30** ($P6_3/mmc$) | **UiO-66** ($Fm$-3m) |
|---|---|

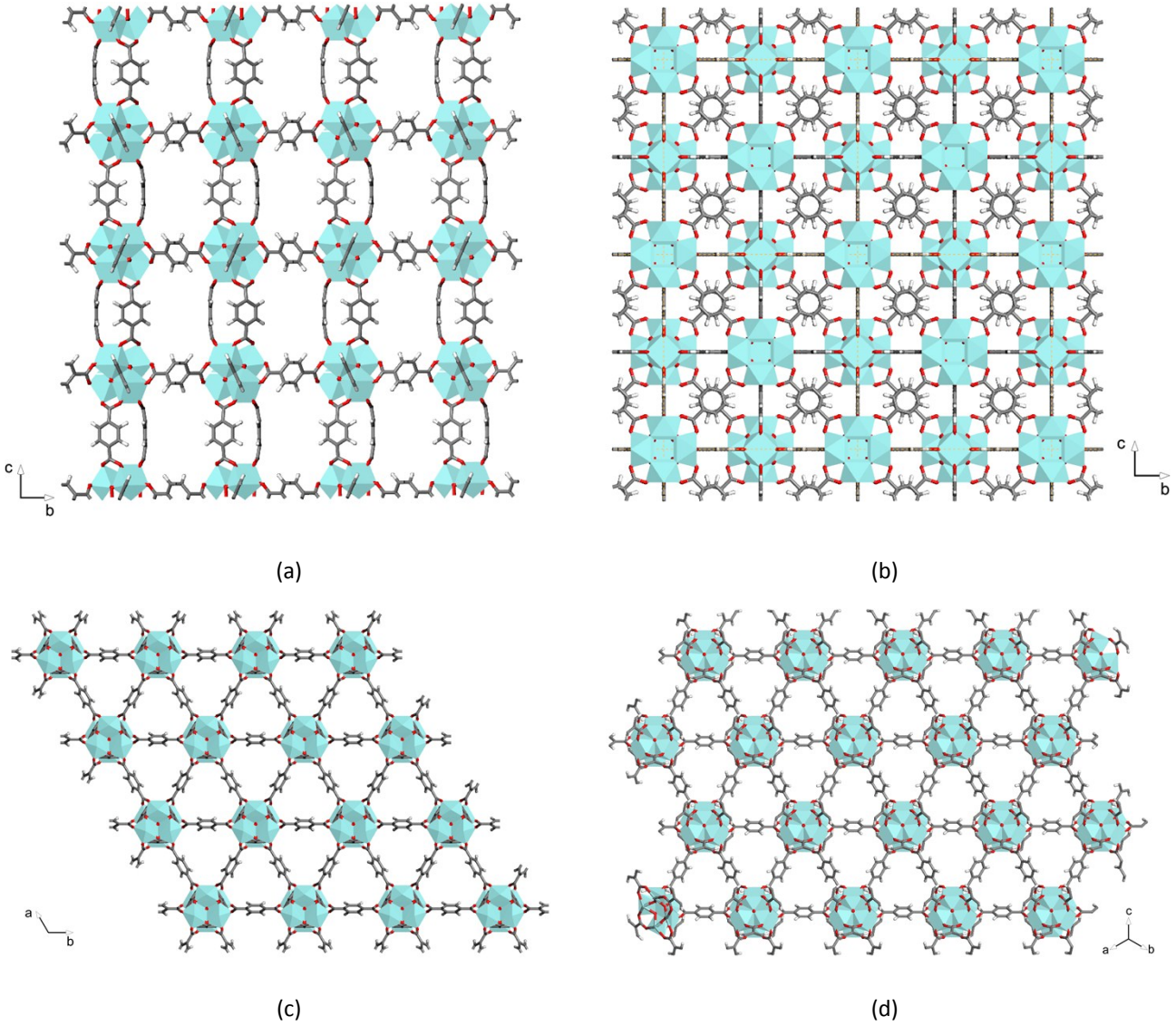


**Figure S3.1**. (a, b) Crystal packing views of EHU-30 and UiO-66 along [100] crystallographic direction. (c, d) Bidimensional hexagonal subnets (**hxl**) of EHU-30 and Uio-66 in which six of the BDC ligands are linking six coplanar Zr-SBUs.

| **EHU-30** ($P6_3/mmc$) | **UiO-66** ($Fm$-3m) |
|---|---|

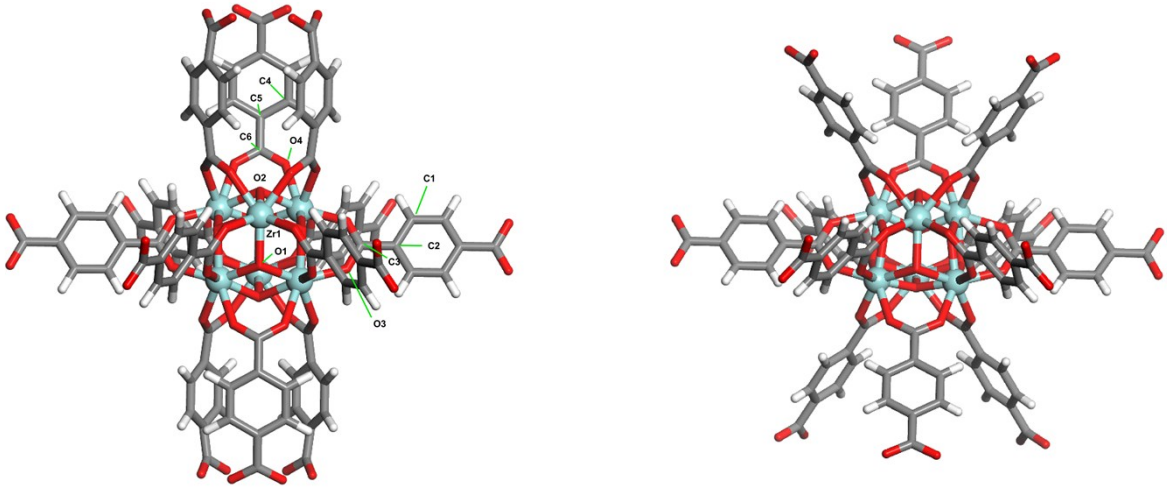


(a) (b)

**Figure S3.2**. (a, b) Coordination environment around the SBUs comprising EHU-30 and UiO-66. It deserves to note that within the inorganic cluster of EHU-30, O2-atom lies at a site with 3m symmetry, while Zr1 and O1 are placed at a general position. In the case of UiO-66, all O-atoms of the inorganic cluster are crystallographically equivalent and are located at threefold symmetry sites. Worthy to mention that the asymmetric unit comprises a zirconium atom, an O1 atom, 1/6 O2 atom (3m site), and a quarter for each of the two crystallographically independent benzene-1,4-dicarboxylato ligands, (mm2 and 2/m, respectively).

## S4. COMPUTATIONAL DETAILS

## S4. COMPUTATIONAL DETAILS

### Simulation of adsorption isotherms

Simulated $N_2$ adsorption isotherms were calculated from a Force-field based Grand Canonical Monte Carlo (GCMC) routine using the SORPTION module included in the BIOVIA Materials Studio 2017 R2 (17.2.0.1626) package. The GCMC simulations were performed using 2 million equilibration steps and 4 million production steps. Both dispersive and electrostatic interactions were taken into account. A Lennard-Jones 12–6 potential was used to model dispersive interactions. The parameters corresponding to atom-atom interactions were estimated by Lorentz-Berthelot mixing rules. A cutoff radius of 12.5 Å was employed for dispersive interactions. In order to model the electrostatic interactions, point charges were assigned to each atom and Ewald summation was used to consider the periodicity of the simulation box.

The Lennard-Jones parameters used to model the fluid molecules ($N_2$) were taken from the TraPPE model ($r_0$ = 3.7153 Å; $D_0$ = 0.2993 kJ·mol$^{-1}$)[11]. This model (Figure S4.1) simulates the quadrupolar moment of the $N_2$ by placing two negative charges (–0.482 e) in the positions of the nitrogen atoms and a positive one in the centre of mass (+0.964 e).

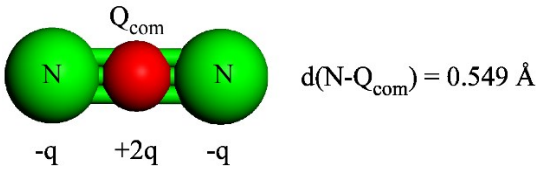


**Figure S4.1.** Model of the $N_2$ molecule used in the GCMC simulation.

The adsorbent structures were built using the crystallographic data of EHU-30 (this work) and UiO-66 (CSD code: *RUBTAK*). Non-located hydrogen atoms corresponding to the hydroxide bridges were added geometrically. The Lennard-Jones parameters for the atoms of the adsorbents (UiO-66 and EHU-30) were taken from the universal force field (UFF).[12] The point charges to model the electrostatic potential of the adsorbents were previously calculated by means of Density Functional Theory (DFT) calculations using the ESP method as described by Singh and Kollman,[13] which is implemented in the DMOL3 code.[14] To accomplish the DFT calculations DNP basis set and the PBE exchange-correlation functional were employed.[15] To conduct the ESP charge calculations neutral finite cluster models of formula $[Zr_6O_4(OH)_4(HBDC)_{12}]$ were built for each MOF. Table S4.1 shows the values of the computed charges.

[11] J. J. Potoff and J. I. Siepmann, *AlChE J.*, 2001, **47**, 1676.

[12] A. K. Rappe, C. J. Casewit, K. S. Colwell, W. A. Goddard and W. M. Skiff, *J. Am. Chem. Soc.*, 1992, **114**, 10024.

[13] U. C. Singh and P. A. Kollman, *J. Comput. Chem*., 1984, **5**, 129.

[14] B. Delley, *J. Chem. Phys*., 2000, **113**, 7756

[15] J. P. Perdew, K. Burke and M. Ernzerhof, *Phys. Rev. Lett.*, 1996, **77**, 3865.

**Table S4.1.** ESP charges (q / e) for the atoms of the structural models of the adsorbents.

| **EHU-30** | | | |
|---|---|---|---|
| Cluster | | Bridging BDC | |
| atom | charge | atom | charge |
| Zr1 | 2.16567 | C1 | -0.236328 |
| O1 | -0.686328 | H1 | 0.128672 |
| O2 | -0.216328 | C2 | -0.0103279 |
| $O1_{(OH)}$ | -0.686328 | C3 | 0.474672 |
| $H1_{(OH)}$ | 0.838044 | O3 | -0.724328 |
| $O2_{(OH)}$ | -0.216328 | | |
| $H2_{(OH)}$ | 0.804017 | | |
| Bridging BDC (triad) | | | |
| atom | charge | atom | charge |
| C4 | -0.130328 | C6 | 0.300672 |
| H4 | 0.0616721 | O4 | -0.427328 |
| C5 | -0.139328 | | |
| **UiO-66** | | | |
| Cluster | | Bridging BDC | |
| atom | charge | atom | charge |
| Zr1 | 2.589090 | C1 | 0.861088 |
| O2 | -1.037910 | C2 | -0.152912 |
| $O2_{(OH)}$ | -1.594910 | C3 | -0.086412 |
| $H2_{(OH)}$ | 0.580088 | H3 | 0.153088 |
| | | O1 | -0.725912 |

**Periodic DFT calculations**

Periodic density-functional theory calculations were conducted by means of the code CASTEP, which uses a plane-wave basis set and pseudopotentials.[16] To accomplish the calculations a plane-wave cut-off of 380 eV and ultrasoft pseudopotentials were selected. The PBE exchange-correlation functional was used in the calculations. The structural models were built using the crystallographic data of EHU-30 (this work) and UiO-66 (CSD code: *RUBTAK*). Non-located hydrogen atoms corresponding to the hydroxide bridges were added geometrically. To save computational time, the calculations were carried out for the converted primitive cells, using one k-point located at the $\Gamma$-point.

[16] I. J. Probert, K. Refson and M. C. Payne, *Z. Kristallogr.*, 2005, **220**, 567.

## S5. GAS ADSORPTION DATA

## S5. GAS ADSORPTION DATA

**BET fitting of simulated and experimental isotherms**

The surface area values were calculated by fitting the adsorption data to Brunauer-Emmett-Teller (BET) equation S4.1:[17]

$$\frac{P/P_0}{V(1-P/P_0)} = \frac{1}{V_M C} + \frac{C-1}{V_M C}(P/P_0) \qquad \text{Equation S4.1}$$

where V is the specific amount adsorbed at the relative pressure $P/P_0$, $V_m$ is the specific amount adsorbed corresponding to the monolayer formation and C is a parameter exponentially related to the energy of monolayer formation.

Regarding the application of the BET method to microporous materials,[18] to avoid ambiguity when reporting the surface area of microporous MOFs, the pressure range for the data fitting was set according the consistency criteria proposed by Roquerol et al.:[19]

(1) The pressure range selected should have values of $V(1 - P/P_0)$ increasing with $P/P_0$.

(2) The points used to calculate the BET surface area must be linear with an upward slope in such a way that the linear regression must yield a positive y-intercept (i.e. positive C value).

(3) The $P/P_0$ value corresponding to $V_m$ should be within the BET fitting range.

Note that the BET surface area calculated from a Type I isotherm must not be considered as a real accessible surface area,[20] but it must be taken as an apparent surface area. In any case, the above described criteria allows to estimate an area that can be regarded as an useful adsorbent "fingerprint", as it avoids a doubtful selection of the fitting range. In fact, this procedure is commonly applied to calculate the BET surface area values of MOFs.[21]

According to the aforementioned first consistency criteria, $V(1 - P/P_0)$ vs $P/P_0$ plots (Figure S5.1) were used to define the pressure range. Second and third criteria were as well fulfilled upon selected fitting range. Resulting BET fitting data are gathered in Table S5.1.

[17] S. Brunauer, P. H. Emmett and E. J. Teller, *Am. Chem. Soc.*, 1938, **60**, 309.

[18] M. Thommes, K. Kaneko, A. V. Neimark, J. P. Oliver, F. Rodriguez-Reinoso, J. Rouquerol and K. S. W. Sing, *Pure Appl. Chem.*, 2015, **87**, 1051.

[19] J. Rouquerol, P. Llewellyn and F. Rouquerol, *Stud. Surf. Sci. Catal*., 2007, **160**.

[20] D. A. Gómez-Gualdrón, P. Z. Moghadam, J. T. Hupp, O. K. Farha and R. Q. Snurr, *J. Am. Chem. Soc.*, 2016, **138**, 215.

[21] (a) O. K. Farha, A. O. Yazaydin, I. Eryazici, C. D. Malliakas, B. G. Hauser, M. G. Kanatzidis, S. T. Nguyen, R. Q. Snurr and J. T. Hupp, *Nat. Chem.*, 2010, **2**, 944; (b) H. Furukawa, N. Ko, Y. B. Go, N. Aratani, S. B. Choi, E. Choi, A. O. Yazaydin, R. Q. Snurr, M. O´Keeffe, J. Kim and O. M. Yaghi, *Science*, 2010, **329**, 424; (c) O. K. Farha, I. Eryazici, N. C. Jeong, B. G. Hauser, C. E. Wilmer, A. A. Sarjeant, R. Q. Snurr, S. T. Nguyen, A. O. Yazaydin and J. T. Hupp, *J. Am. Chem. Soc.*, 2012, **134**, 15016; (d) K. S. Walton and R. Q. Snurr, *J. Am. Chem. Soc.*, 2007, **127**, 8552.

**Table S5.1**. BET fitting details for experimental and simulated $N_2$ isotherms.

| Code | $P/P_0$ range | $S_{BET}$ ($m^2/g$) | $R^2$ | C | $V_m$ ($cm^3/g$) | $P/P_0$ for $V_m$ (interpolation) |
|---|---|---|---|---|---|---|
| **EHU-30** Experimental | 0.0009 – 0.0304 | 1015 | 0.99999 | 5838.8 | 233.10 | 0.01368 |
| **EHU-30** Simulation | 0.0002 – 0.0053 | 1399 | 0.99999 | 237757 | 321.16 | 0.00170 |
| **UiO-66** Simulation | 0.0002 – 0.0053 | 1283 | 0.99999 | 227638 | 294.61 | 0.00201 |

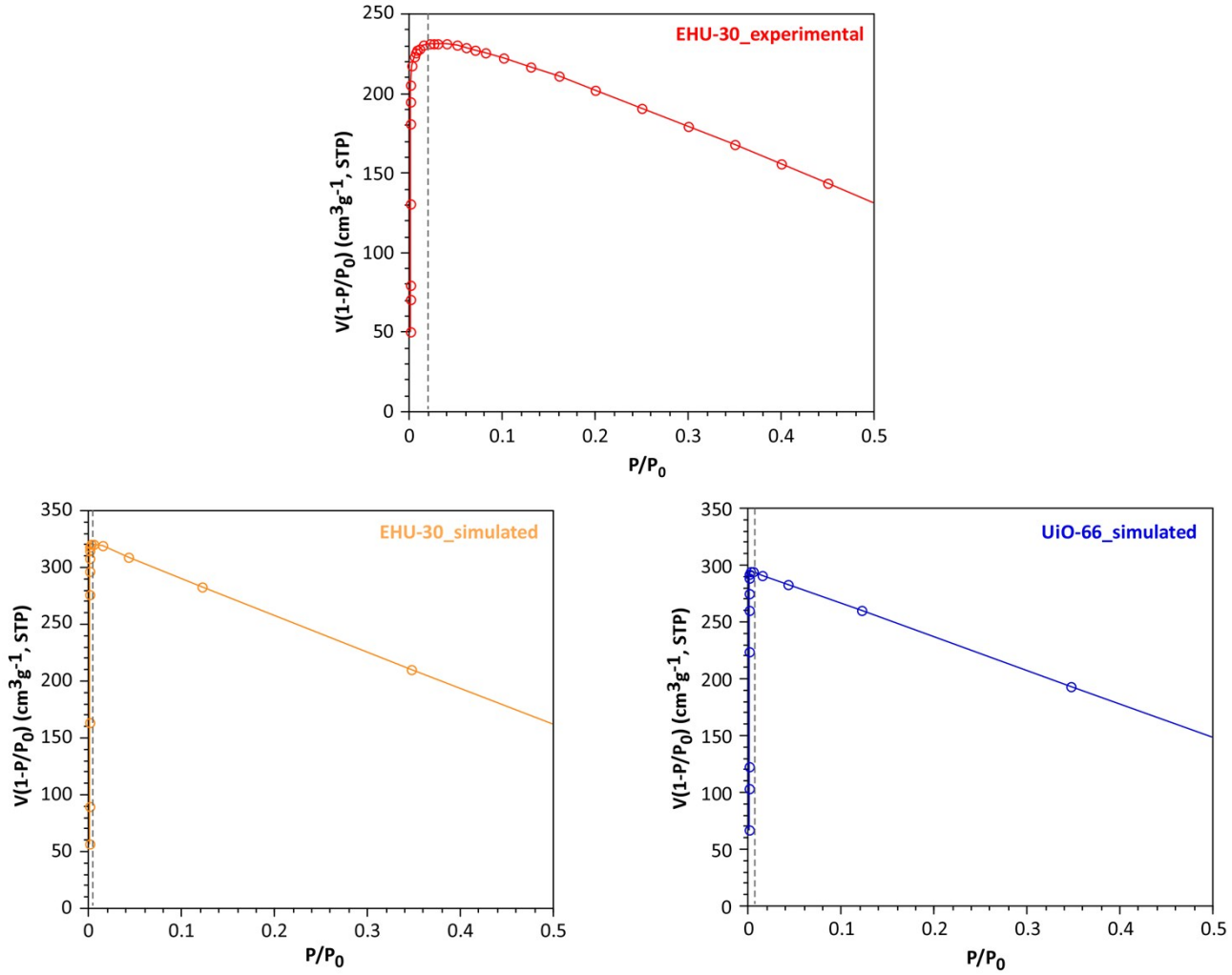


**Figure S5.1.** Consistency plot [$V(1 - P/P_0)$ vs. $P/P_0$] for experimental and simulated $N_2$ isotherms.

## $CO_2$ adsorption isotherms and calculation of isosteric heats of adsorption

$CO_2$ adsorption isotherms were measured at 273 and 298 K for EHU-30 sample (Figure S5.2a). In order to estimate $CO_2$ adsorption enthalpies ($Q_{st}$), the isotherms were fitted to modified Clausius–Clapeyron equation.[22] Resulting data are gathered in Figure S5.2b.

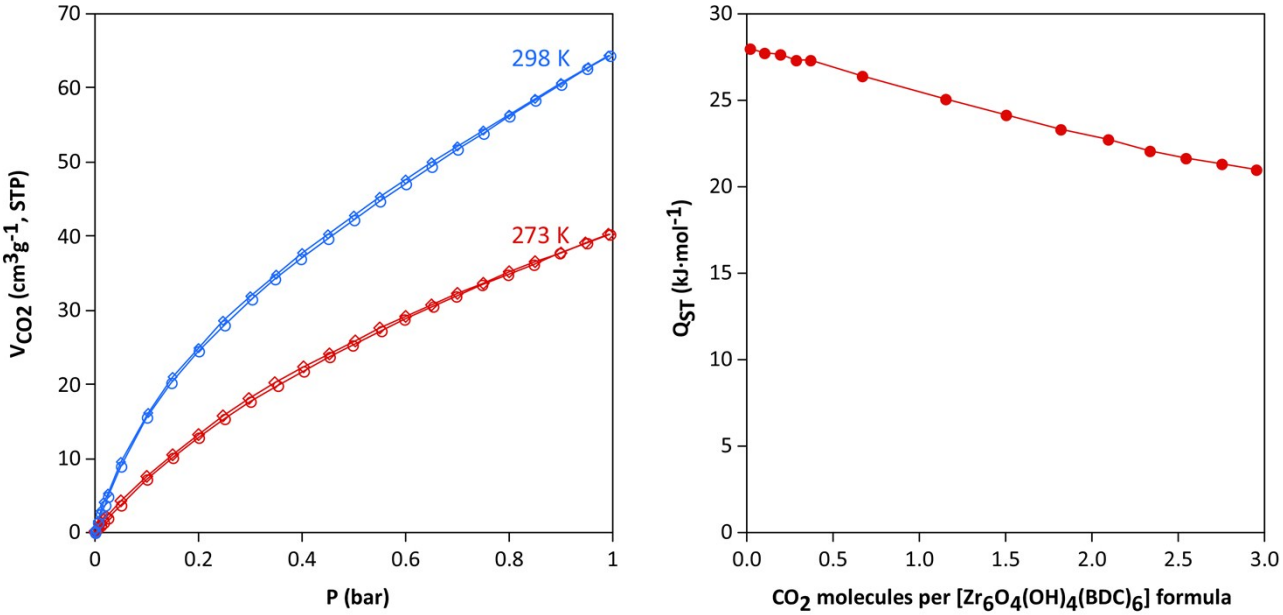


**Figure S5.2.** (a) $CO_2$ adsorption isotherms at 273 and 298 K measured upon EHU-30 sample (circles and diamonds stand for adsorption and desorption branches, respectively) (b) calculated isosteric heats of adsorption for $CO_2$.

[22] (a) K. Sumida, D. L. Rogow, J. A. Mason, T. M. McDonald, E. D. Bloch, Z. R. Herm, T-H. Bae and J. R. Long, *Chem. Rev.*, 2012, **112**, 724; (b) H. Pan, J. A. Ritter and P. B. Balbuena, *Langmuir*, 1998, **14**, 6323.